View metadata, citation and similar papers at core.ac.uk

brought to you by CORE

provided by University of Bath Research Portal

Citation for published version:
Young, A, Turner, J & Head, R 2021, 'Turbocompounding the Opposed-Piston 2-Stroke Engine', Paper presented at SAE 2021 World Congress, Detroit, USA United States, 13/04/21 - 15/04/21.

Publication date:
2021

Link to publication

Publisher Rights
Unspecified

University of Bath

Alternative formats
If you require this document in an alternative format, please contact:
openaccess@bath.ac.uk

General rights
Copyright and moral rights for the publications made accessible in the public portal are retained by the authors and/or other copyright owners and it is a condition of accessing publications that users recognise and abide by the legal requirements associated with these rights.

Take down policy
If you believe that this document breaches copyright please contact us providing details, and we will remove access to the work immediately and investigate your claim.

Download date: 11. May. 2021

Turbocompounding the Opposed-Piston 2-Stroke Engine

Author, co-author (Do NOT enter this information. It will be pulled from participant tab in MyTechZone)

Affiliation (Do NOT enter this information. It will be pulled from participant tab in MyTechZone)

Abstract

This paper presents analytical research conducted into the level of fuel consumption improvement that can be expected from turbocompounding a medium-duty opposed-piston 2-stroke engine, which is part of a hybridized vehicle propulsion system. It draws on a successful earlier study which showed a non-compounded opposed-piston engine to be clearly superior to other forms of 2-stroke engine, such as the widely adopted uniflow-scavenged poppet valve configuration. Electrical power transmission is proposed as the method of providing the necessary variable-speed drive to transmit excess turbine power to the system energy storage medium. The work employs one-dimensional engine simulation on a single-cylinder basis, using brake specific fuel consumption (BSFC) as the reportable metric, coupled with positive or negative power flow to the engine from the compounder; this is a variation on an approach successfully used in earlier work. Here it shows the sensitivities of the overall system to cylinder pressure, the compressor and turbine efficiencies, exhaust backpressure and also provides a means to investigate the effect of the power transmission efficiency on the overall benefit. Reheating the air before the turbine is also investigated as a means of providing a "burst" performance facility, albeit at the expense of extra fuel consumption. Positive compounding work is shown to be achievable across all investigated engine operating points under certain conditions. Operating points at lower engine speeds showed an increased propensity for turbocompounding, with 5-6% of the brake torque arising from the compounder, compared to those at higher engine speeds, where a maximum of 4% was seen. BSFC was found to be highly dependent on compounding torque with improvements only arising from reducing backpressure. A better understanding of the flow restrictions of the exhaust aftertreatment and muffler systems, for a given application, would allow for more accurate determination of the possibility for BSFC reduction within realistic operating conditions.

Introduction

Opposed-Piston Engines

The opposed-piston 2-stroke (OP2S) engine has historically been applied to aircraft propulsion as well as engines for power generation and rail traction with great success [1, 2, 3]. More recently, Achates Power have shown the potential of the OP2S engine for automotive applications [4, 5, 6, 7]. In part due to its lack of a cylinder head, the OP2S engine has relatively low heat loss from the combustion gas, instead maintaining the energy in the exhaust gas. This makes it an ideal candidate for turbocharging, as it allows further useful work to be extracted from the high energy exhaust gases. However, due to the requirement for a positive delta pressure across the cylinder (intake manifold pressure must be higher than exhaust manifold pressure) for the scavenging performance of all 2-stroke engines, some form of system to provide the necessary pressure gradient is required for OP2S engines. It is for this reason that a supercharger may typically be used in conjunction with a turbocharger, to ensure the positive delta pressure at all operating points of the engine [4]. Historically, OP2S engines have been turbo-compounded with success (where the crankshaft is linked to the compounder, or turboshaft, with a variable-speed drive), not only allowing the turbocharger to act as a supercharger when required but also providing a means for utilization of excess turbine work [8, 9, 10].

Turbocompounding

Turbocompounding is primarily used as a form of waste heat recovery system for internal combustion engines. In turbocharged engines, excess turbine work is typically wasted by means of a wastegate or dump valve. Turbocompounding provides a means of utilizing that excess work to increase the work output from the engine crankshaft [11]. Historically, the necessary variable-speed drive between the compounder and the engine has been mechanical [9, 10], however, modern turbocompounding systems utilize electrical power transmission [12, 13].

Turbine power can be defined as:

$$P = \eta_T \dot{m} C_p T_{0,in} \left[1 - \left(\frac{p_{out}}{p_{0,in}} \right)^{(\gamma-1)/\gamma} \right] \quad (1)$$

where $\eta_T, \dot{m}, C_p, T_{0,in}, p_{out}, p_{0,in}, \gamma$ are turbine isentropic efficiency, exhaust mass flow rate, specific heat capacity of exhaust gases at constant pressure, turbine inlet total temperature, turbine outlet static pressure, turbine inlet total pressure and specific heat ratio, respectively. From analysis of equation 1, it can be seen that the inlet total pressure has the greatest effect on turbine output power. A reduction in outlet static pressure yields an increase in turbine power, however, an equal pressure change exhibited at the intake side generates a larger work increase. Furthermore, the mass flow rate of the exhaust gases along with the turbine inlet total temperature are directly proportional to turbine power. This demonstrates that, in order to maximize turbine work, either the turbine expansion ratio must be increased, or the inlet total temperature or mass flow rate of the exhaust gases must be increased. This gives rise to the reasonings for reheating the air before the turbine, as it can be seen to have a direct effect on the output power of the turbine.

Methodology

Throughout this work, the suitability of turbocompounding the OP2S engine is assessed at two engine speeds, 1500 rpm and 3000 rpm, notionally representing the engine speeds for peak torque and peak power respectively. This is achieved by analyzing the interaction between brake engine torque, compounding torque and brake specific fuel consumption before assessing how they respond to variation of turbomachinery efficiencies, reheat and backpressure. The basis of the formulation of the OP2S engine model in this study initiated from previous work carried out in a joint study of 2-stroke scavenging systems conducted by the University of Bath and Aramco in 2018 [14]. The engine geometries, port timings and scavenging utilized in the OP2S model were carried forward into this work, with alterations being made in order to assess the suitability of turbocompounding the engine.

Table 1. Summary of the modelled OP2S engine specifications.

Basic Scavenging System	Uniflow
Bore [mm]	75.75
Stroke [mm]	166.65
Cylinder Volume [cc]	751.04
Stroke:Bore ratio	2.2
Conrod Length [mm]	166.65
Compression Ratio	15:1
Exhaust Piston Lead [CAD]	7.5

The model consists of a single cylinder with simplified external air path geometries, modelled in GT-Power - a 1-D engine simulation software package. A summary of the modelled OP2S engine specifications is shown in Table 1. The opposed piston cylinder is represented as an equivalent single piston cylinder of stroke equal to the total stroke of the two opposed pistons with a single piston head area the total size of the two piston heads combined. The motion of this equivalent piston mimics the motion of the exhaust piston 'as seen' from the intake piston. In opposed piston engines, the exhaust piston typically 'leads' the intake piston by 5-10 degrees; this is accounted for in the model and can be varied if desired. Throughout this work, the exhaust piston lead is set to 7.5 crank angle degrees (CAD). The piston ported valve events are simulated by overriding the flow area multiplier of a standard ported valve connection. The crank angle is used to calculate the respective positions of the intake and exhaust pistons, which are then used to calculate the open port areas, at said given crank angle. The combustion heat release profile used in the previous model, shown in Figure 1, was adopted from prior work by Aramco on gasoline compression ignition (GCI) [14, 15]. The scavenging profile for the original OP2S engine model, taken from work by Mattarelli et al. [16], can be seen in Figure 2. These were both utilized in all simulations throughout this work.

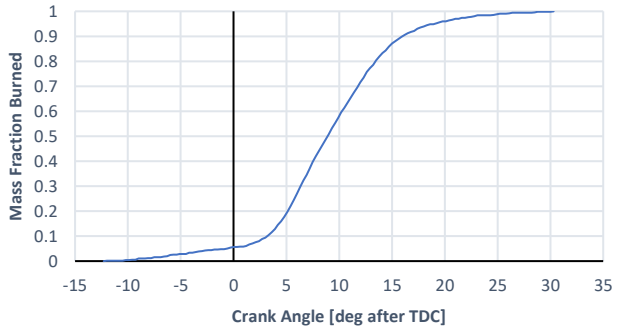

Figure 1. Combustion heat release profile adopted from previous work performed by Aramco on GCI [15].

Figure 3 shows a schematic representation of the engine configuration modelled in this work. The turbocompounding is provided by an e-turbocharger (a turbocharger with an electric machine mechanically linked to the turboshaft), electrically coupled to another electric motor, which is mechanically linked to the crankshaft. This simplified electrical arrangement, combined with fixed electromechanical conversion efficiencies of 95% for each motor, allows for evaluation of the combined engine and turbocompounding system. As only one cylinder, without meaningful external air path geometries, is being modelled, the turbomachinery model is simply two single-stage adiabatic expansion/compression equations, one each for the turbine and compressor respectively. An isentropic efficiency is defined for each stage, a sensitivity study for which was undertaken. The turboshaft mechanical efficiency is set at 98%.

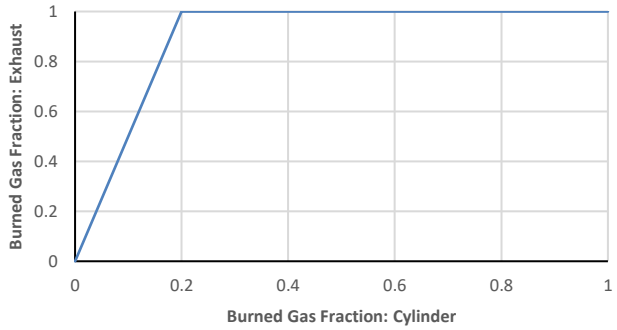

Figure 2. Scavenge profile used for the OP2S engine configuration, taken from work by Mattarelli et al. [16].

A pre-turbine catalyst is utilized for increased exhaust aftertreatment performance whilst maximizing the potential work extraction from the exhaust gases. Close-coupled catalysts have been shown to improve conversion efficiency during steady state conditions whilst also decreasing catalytic light-off time [17, 18], resulting in a combined beneficial effect on total emissions. Moreover, assuming that a catalyst would exhibit the same pressure drop whether it was pre- or post-turbine, the turbine expansion ratio will be larger should this pressure drop occur pre-turbine (compared to post-turbine), yielding greater turbine work extraction. Throughout this work, as the determination of the individual flow restrictions of each catalyst was deemed out of scope, the pressure drops of the close coupled pre-turbine catalyst and the post-turbine aftertreatment system were combined and assumed to occur downstream of the turbine. However, as the estimated turbine work extraction would be larger if the individual pressure drops were

separately modelled and occurred in their respective places, this assumption is deemed viable as the results can be seen as a worst-case scenario. Furthermore, the use of a pre-turbine catalyst also allows for the creation of an integrated catalytic reheat chamber. The purpose of which is to use catalytic combustion with the excess oxygen in the exhaust, present due to the lean burn operation of the OP2S engine, to increase the gas temperature and thus increase the turbine work extraction. Though this is predicted to disproportionately increase the BSFC by yielding moderate gains in torque for a relatively large quantity of burned fuel, it is presented here as an investigation into its potential for use as a temporary boost function.

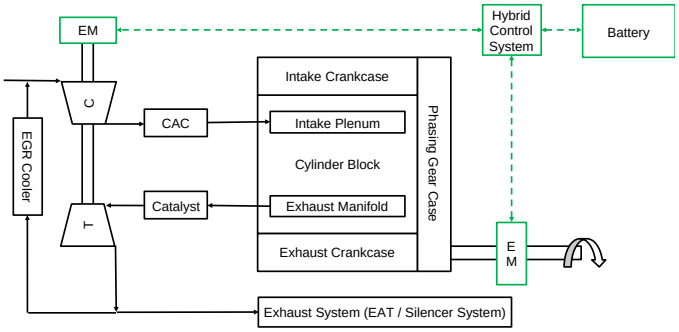

Figure 3. Schematic representation of the OP2S engine configuration with an e-turbocharger (left) providing the compounding, using electrical power transmission as the method of variable-speed drive. CAC: charge air cooler; EGR: exhaust gas recirculation; EM: electric machine; EAT: exhaust aftertreatment.

The use of a low-pressure exhaust gas recirculation (EGR) system allows the turbine to extract energy from the exhaust gases prior to recirculation. This increases the possible turbine work whilst also reducing the required power of the EGR cooler, due to the lower inlet gas temperature. Furthermore, due to the pre-turbine catalyst, the EGR occurs post-catalyst which has been shown to be beneficial for decreasing autoignition potential due to the reduction in free radical species that are known to initiate chain reactions [19]. The increased ignition delay caused by this could allow for greater in-cylinder charge mixing pre-combustion, improving combustion efficiency and reducing emissions production.

Validation

Once the new model was constructed with the necessary changes required for analysis of turbocompounding, verification was undertaken to ensure the validity of the model. This was achieved by ensuring that the new model would output similar results to the previous model when given the same input values. The previous model used a PID controller to target a specific indicated mean effective pressure (IMEP) value by allowing it to vary the post-compressor pressure. The converged post-compressor value from the controller, along with the pre-turbine pressure that was set in the previous model, were both set in the new model. The pre-compressor pressure was assumed to be 1 bar absolute whilst the post-turbine pressure was estimated by assuming the pressure drop across the exhaust aftertreatment and muffler system would vary with the square of volumetric exhaust flow rate.

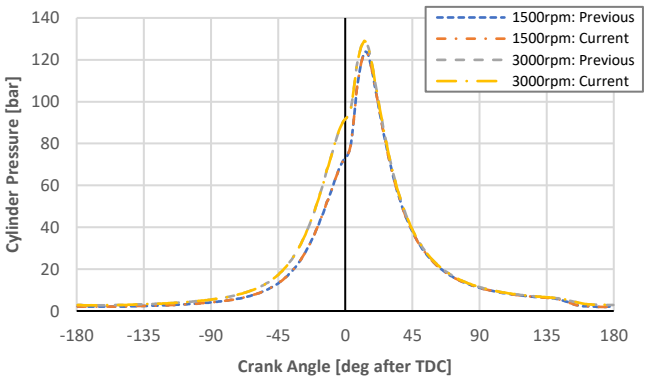

Figure 4. Comparison of the in-cylinder pressure traces from the previous and current models under a full load condition at 1500 rpm and 3000 rpm for verification purposes.

Figure 4 shows a comparison of the cylinder pressure traces for both the previous and current models, at 1500 rpm and 3000 rpm, under the operating conditions discussed above. No discernable difference in the cylinder pressure traces can be seen between the two models. In fact, the maximum cylinder pressure percentage error between the two models were 0.0005% for 1500 rpm and 0.02% for 3000 rpm. Most other parameters (such as IMEP, torque, fuel consumption, etc.) were equal between the two models to at least four significant figures. Therefore, as the new model has been shown to produce repeatable results from prior published work, it is taken to be validated.

Development of the Model

Once the new model was validated against the previous model, further work was undertaken to improve the new model in an attempt to combat some of the limitations that the previous model possessed, as a result of it being part of a study to investigate six different scavenging systems. Firstly, the direct fuel injection in the previous model occurs shortly after intake port closure, whilst the pre-set combustion heat release profile occurs at a fixed point, around top dead center. Whilst acceptable in the previous study, this is unrepresentative of what would occur in practice as the ignition delay is highly dependent on various factors, such as cylinder temperature and pressure. In order to improve this in the new model, an ignition controller was added. A desired 50% burned crank angle is set as an input variable which fixes the start of the combustion heat release profile. It is initially assumed that the start of injection (SOI) occurs at the same time as the start of combustion heat release. The simulation is then run with the cylinder temperature at the SOI being used to calculate the ignition delay (defined as the time between the SOI and the 50% burned point). Data from multiple sources was used to formulate an equation relating ignition delay to cylinder temperature at SOI [20, 21, 22, 23, 24]. The calculated ignition delay is then used to set a new SOI point. The simulation is then run again with this new SOI point, with the cylinder temperature at that crank angle once again being used to determine the ignition delay, before calculating a new SOI point. As the simulation runs, this controller converges on a SOI crank angle that would feasibly yield the desired 50% burned crank angle set initially. The aforementioned fuel injection timing controller allows for control over the compression ignition event simply by setting the desired 50% burned crank angle.

Secondly, the previous model did not include any friction approximation; consequently, the prior work presented results on an indicated basis. Without a prediction of engine friction, it is not only difficult to draw accurate comparisons between different engine

operating conditions but also difficult to evaluate the overall performance of the engine when compared to other configurations. Therefore, a Chen-Flynn friction model was created within the engine model. The model was parameterized, using the recommended methodology outlined in the GT-Suite manuals, to match friction mean effective pressure (FMEP) values typical of this style of OP2S engine, from the authors' experience.

In order to model the effects of the aforementioned reheat chamber, the mass fraction of oxygen in the exhaust, coupled with the exhaust mass flow rate, were used to determine the fuel mass flow rate required to yield stoichiometric combustion products. The gas temperature rise caused by the catalytic combustion of the calculated fuel mass was added to the existing exhaust gas temperature before being used to calculate the new increased turbine work extraction. A temperature limit of 1273K was set for turbine protection. If the newly calculated exhaust gas temperature was greater than this limit, the quantity of fuel required to achieve 1273K was calculated and used instead. The effects of this secondary combustion event on the specific heat (c_p) and specific heat ratio (γ) of the exhaust gases were estimated before each turbine work calculation. The finalized fuel mass flow rate for the reheat combustion was then combined with the existing cylinder fuel mass flow rate before calculation of the new BSFC.

Optimizer Set-up

Before evaluation of the effects of turbomachinery efficiencies, reheat and backpressure could be assessed, operating points for the engine needed to be determined. Due to the large state space of feasible engine operation, the integrated design optimizer within GT-Suite was used to implement a multi-objective Pareto optimization utilizing a genetic search algorithm. The optimizer requires three main things to be defined: the input variables and their bounds; the constraints; and the desired target objectives. The target objectives were set to minimize BSFC whilst maximizing brake torque and compounding torque. The process of setting the constraints and the input variables is discussed below.

Setting Constraints

It is important to constrain the optimizer appropriately as it will ensure the feasibility and comparability of the simulation results. Firstly, as the production of engine emissions are highly dependent on cylinder temperatures during combustion, limits on the peak cylinder temperature have been imposed. Cylinder temperatures lower than 1400K have been shown to lead to incomplete combustion, yielding increased hydrocarbon (HC) emissions, whilst cylinder temperatures higher than 2200K lead to increased NOx formation [21]. Therefore, the first constraint imposed on the optimizer is that the peak cylinder temperature must be in the range 1600K to 2200K.

Another factor that is crucial to limit within the model is the peak cylinder pressure. Setting the peak cylinder pressure is primarily an engine design constraint; the pistons, piston rings, connecting rods, crankshaft, bearings, etc. will all be specified to withstand the forces that the chosen maximum cylinder pressure will exert on the system. However, as these components are uprated to withstand higher forces, they typically also become heavier, larger and more costly whilst yielding increased friction and rotational inertia. This, in turn, increases the overall size, weight and cost of the engine.

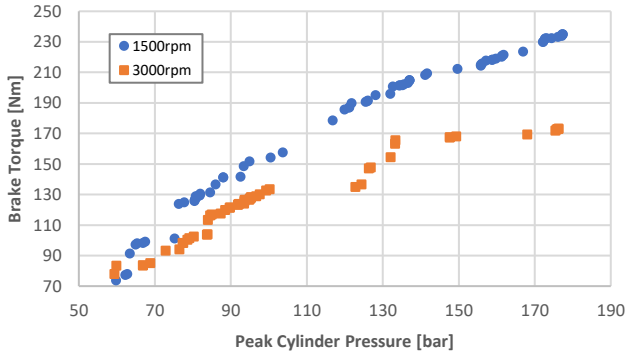

Figure 5. Variation of maximum achievable brake torque with peak cylinder pressure at 1500 rpm and 3000 rpm.

The effect of varying the allowable peak cylinder pressure on the maximum achievable torque generated by the model can be seen in Figure 5. Understandably, there is initially a linear relationship between the two variables at each engine speed. At higher pressures the peak cylinder pressure will no longer be the limiting factor, causing the relationship to plateau. It can be seen that this has a greater effect on the maximum achievable torque at the higher engine speed of 3000rpm. The effect is more slight at 1500rpm due to the higher allowable cylinder pressure rise rates. A similar OP2S engine from Achates is specified to operate up to 220 bar peak cylinder pressure due to advances in wrist pin technology [25], a known limitation for 2 stroke engines operating with peak cylinder pressures above 150 bar. For the purpose of this work, the peak cylinder pressure was arbitrarily at 165 bar, though it is the authors' beliefs that a higher peak cylinder pressure could be possible.

However, limiting peak cylinder pressure does not ensure that the combustion will proceed without damaging byproducts, such as engine knocking. Although many factors affect the potential for engine knocking, limiting the maximum pressure rise rate (MPRR) is known to highly reduce the propensity. The absolute MPRR values known to cause knocking combustion are in the range 5-12 bar/CAD, decreasing with engine speed [22]. Therefore, it could be appropriate to express the rate of pressure rise with respect to time, rather than CAD, as done by Yoshizawa et al. [26], where an allowable MPRR of 50 bar/ms is discussed. Furthermore, a MPRR value of around 5 to 6 bar per CAD is often used as a noise, vibration and harshness (NVH) limit as, beyond this, the audible rattle is deemed unsuitable for some automotive applications. However, the use of pilot fuel injection has been shown to be highly effectively at reducing the MPRR during GCI. Liu et al. [27] show that the MPRR of a given combustion cycle can be reduced from 10.7 bar/CAD to 5.4 bar/CAD when a pilot injection is utilized compared to a single injection strategy; a further benefit shown in the work is a reduction in BSFC when a pilot injection is used. Modelling of pilot injections is deemed beyond the scope of this work; however, it can be assumed that similar effects would be shown had it been included in this work. Therefore, the estimated MPRR reduction deemed feasible by use of a pilot injection scheme is taken into account when setting MPRR constraints. A value of under 5 bar/CAD is believed to be achievable at 1500 rpm with a pilot injection scheme, if the MPRR for a single injection scheme is no more than 10 bar/CAD; a MPRR limit of 10 bar/CAD at 1500 rpm is therefore imposed on the model. Similarly, a MPRR of under 3 bar/CAD is believed to be achievable at 3000 rpm, should the MPRR for a single injection scheme be no more than 6 bar/CAD; a MPRR limit of 6 bar/CAD at 3000 rpm is therefore imposed on the model. The predicted

achievable MPRRs set by these limits correspond to 45 bar/ms and 54 bar/ms for 1500 rpm and 3000 rpm, respectively.

A summary of the three optimizer constraints can be seen in Table 1.

Table 2. Summary of constraints imposed on the optimizer at each engine speed.

Variable	1500 rpm		3000 rpm	
	Min	Max	Min	Max
Peak Cylinder Temperature [K]	1600	2200	1600	2200
Peak Cylinder Pressure [bar]	0	165	0	165
Maximum Pressure Rise Rate [bar/deg]	0	10	0	6

Parameterizing the Input Variables

As the turbomachinery model in this work exists solely as two isentropic equations with efficiencies held constant over the cycle duration, there is no link between gas flow rates and pressure ratios, as would normally be detailed in a compressor/turbine map. Therefore, the pressures at the inlet and outlet of both the compressor and turbine must be defined by the user. The compressor inlet pressure is assumed to be 1 bar absolute, as is the exhaust outlet pressure (downstream of the aftertreatment and muffler systems). The turbine outlet pressure is determined by a calculated pressure differential due to an estimated flow restriction, caused by the aftertreatment and muffler. The compressor outlet pressure, assumed equal to the manifold absolute pressure (MAP), is used as an input variable for the optimizer. The turbine inlet pressure is defined by the compressor outlet pressure minus a variable termed ‘delta pressure’, the second optimizer input variable, which represents the pressure differential across the cylinder. Defining the turbine inlet pressure in this way makes it possible to ensure a positive pressure differential across the cylinder, which is a requirement for 2-stroke engines to scavenge. The air-fuel-ratio (AFR), based on the mass air flow through the intake orifice multiplied by the cylinder trapping ratio, is the third optimizer input variable; a range of 15 to 25 was used for both speeds, corresponding to a global equivalence ratio of about 1 (stoichiometric) and 0.6 (lean) respectively. The percentage of exhaust gases present in the pre-compressor intake air from external exhaust gas recirculation (exclusive of trapped residuals) was allowed to vary between 0% and 40%, forming the fourth optimizer input variable. The final optimizer input variable is the 50% burned crank angle (CA50), defined in CAD after top-dead-center (ATDC), allowing the optimizer to vary the timings of the combustion event. Table 2 shows the five optimizer input variables alongside their respective range values.

Table 3. Summary of the input variables, and their respective ranges, for the optimizer at each engine speed.

Variable	1500 rpm		3000 rpm	
	Min	Max	Min	Max
Intake Pressure [bar]	2	4	3	6
Delta Pressure [bar]	0.2	1.2	0.8	1.8
AFR	15	25	15	25
EGR [%]	0	40	0	40
CA50 ATDC [CAD]	5	25	5	25

Results and Discussion

Operating Points

Figures 6-8 and Figures 9-11 show the results from the optimizer for 1500 rpm and 3000 rpm respectively. Figure 6 plots the generated points for 1500 rpm on a graph of BSFC against brake torque. It can be seen that for a large increase in brake torque (130 Nm to 194 Nm), there is only a very slight increase in BSFC (207 g/kWh to 210 g/kWh). This is believed to be due to lower values of delta pressure (0.35 bar to 0.6 bar) causing comparatively poorer scavenging performance, compared to higher values of delta pressure. This causes less free oxygen to be present in the cylinder, reducing the quantity of fuel that can be combusted and thus injected. This, in turn, allows for an earlier combustion event, within the MPRR constraints, which yields a more efficient combustion process. Also, the lower delta pressure values allow for greater turbine work extraction by virtue of a larger expansion ratio. This increased turbine work will lead to an increase in brake torque, due to the compounding system, for no extra fuel consumption, further aiding the BSFC. Marginally higher torque values (6 Nm increase) can be reached at the expense of BSFC (20 g/kWh increase) as seen in Figure 6. This is believed to be due to higher values of delta pressure (0.75 bar to 1.05 bar) yielding improved scavenging performance, increasing the quantity of fuel that can be combusted and thus injected. Even though this increased quantity of fuel yields greater brake torque, it requires a more retarded combustion event to stay within the confines of the constraints, which yields a less efficient combustion event. This is exacerbated by the decreased turbine work extraction due to the lower expansion ratio caused by the larger delta pressure. This reduces the brake torque for the same fuel consumption, increasing the BSFC.

Figure 7 shows generated points for 1500 rpm on a graph of compounding torque against brake torque. Compounding torque is defined as ‘the torque from the electric compounding system, as seen by the crankshaft’. A positive value indicates that surplus work from the compounding system is being used to increase brake torque; a negative value indicates that work is being taken from the crankshaft, reducing the brake torque, to supply the work deficit in the compounding system (effectively supercharging). Compounding torque can be seen, in Figure 7, to decrease with increased brake torque. This is believed to be due to a larger delta pressure yielding better scavenging, leading to combustion of more fuel, increasing brake torque; However, a larger delta pressure causes less turbine work extraction, leading to decreased compounding torque. Figure 7 almost perfectly mirrors Figure 6, the reason for which can be seen in Figure 8, which plots the generated points for 1500 rpm on a graph of BSFC against compounding torque. It shows that BSFC decreases linearly with increasing compounding torque. This was expected as larger compounding torque values increase brake torque with no increase in fuel consumption, therefore decreasing BSFC.

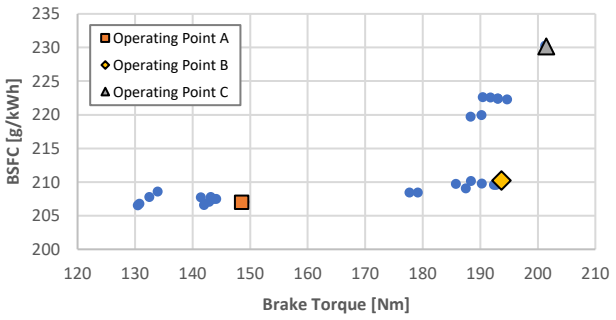

Figure 6. Distribution of optimizer results on a graph of BSFC against brake torque at 1500 rpm with the three chosen operating points identified.

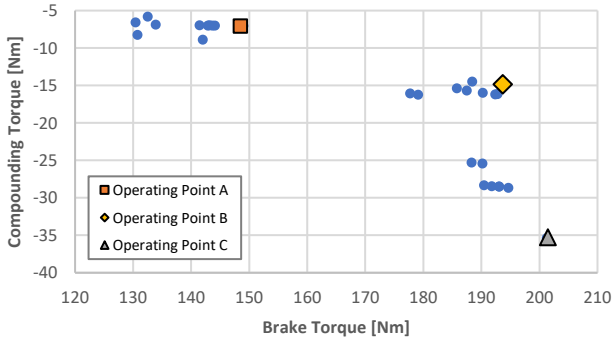

Figure 7. Distribution of optimizer results on a graph of compounding torque against brake torque at 1500 rpm with the three chosen operating points identified.

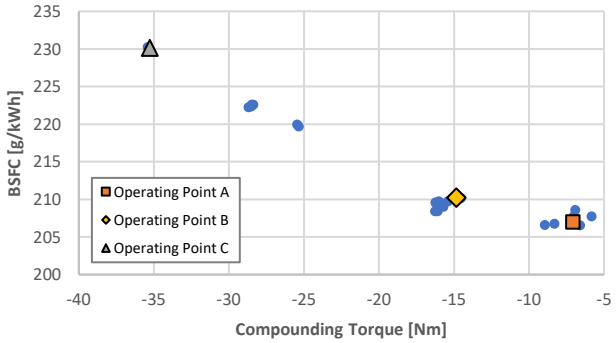

Figure 8. Distribution of optimizer results on a graph of BSFC against compounding torque at 1500 rpm with the three chosen operating points identified.

Figure 9 plots the generated points for 3000 rpm on a graph of BSFC against brake torque. It can be seen that BSFC increases linearly with increased brake torque. This is because the MPRR constraint is causing all of the generated points to have equally retarded combustion events. Increasingly higher intake pressures and delta pressures are required for increased brake torque; however, this causes a decrease in compounding torque, due to the reduced turbine work extraction and increased compressor work required. This can be seen in Figure 10, where a linearly decreasing trend is present in the generated points for 3000 rpm when plotted on a graph of compounding torque against brake torque. In similar fashion to the results for 1500 rpm, Figure 11 shows a linearly decreasing trend in BSFC when plotted against compounding torque.

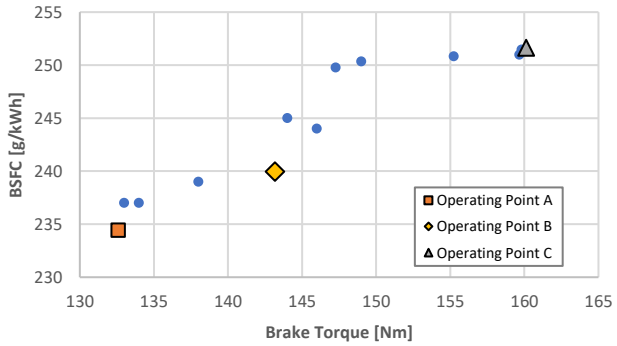

Figure 9. Distribution of optimizer results on a graph of BSFC against brake torque at 3000 rpm with the three chosen operating points identified.

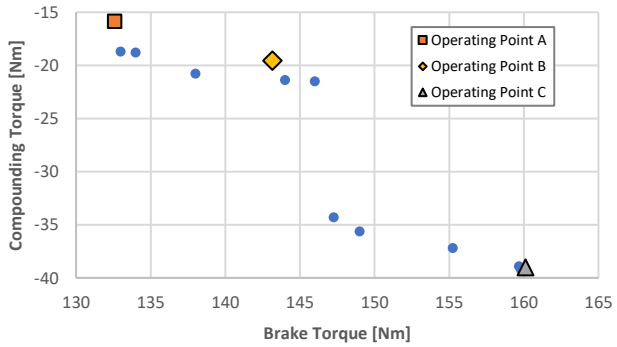

Figure 10. Distribution of optimizer results on a graph of compounding torque against brake torque at 3000 rpm with the three chosen operating points identified.

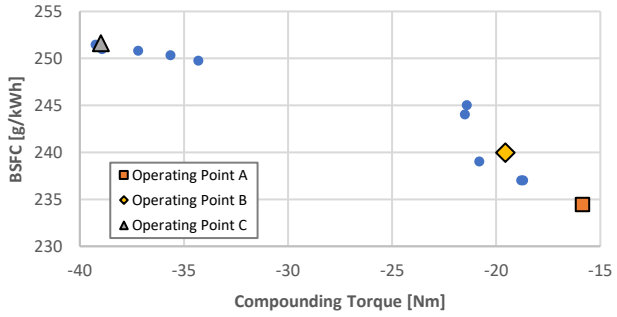

Figure 11. Distribution of optimizer results on a graph of BSFC against compounding torque at 1500 rpm with the three chosen operating points identified.

Throughout Figures 6-8 and Figures 9-11, three operating points (termed A, B and C), for each engine speed, were highlighted. These 3 operating points were selected to represent:

A. High compounding torque
B. Efficiency 'knee'

C. Peak brake torque

These three operating points are used in all subsequent simulations for comparative purposes. A summary of the three chosen operating points for each speed can be seen in Table 3. The first five rows of data show the values of input variables as chosen by the optimizer. The following three rows show the values of each constrained variable. The final four rows display the brake torque, BSFC, compounding torque and brake mean effective pressure (BMEP) for each operating point, respectively.

Table 4. Summary of the three chosen engine operating points at each engine speed.

	1500 rpm			3000 rpm		
Operating Point	**A**	**B**	**C**	**A**	**B**	**C**
Intake Pressure [bar]	2.28	2.88	2.93	3.30	3.54	5.02
Delta Pressure [bar]	0.39	0.56	1.01	1.14	1.28	1.58
AFR	20.2	19.8	19.2	16.8	16.5	19.8
EGR	36%	37%	24%	22%	24%	39%
CA50 ATDC [CAD]	10.4	10.7	13.6	14.9	15.0	15.2
Peak Cylinder Temperature [K]	2070	2110	2190	2170	2170	1980
Peak Cylinder Pressure [bar]	124	161	157	114	122	165
MPRR [bar/deg]	7.09	9.36	9.41	5.10	5.61	5.78
Brake Torque [Nm]	149	194	201	133	143	160
BSFC [g/kWh]	207	210	230	234	240	252
Compounding Torque [Nm]	-7.08	-14.8	-35.3	-15.9	-19.6	-39.0
BMEP [bar]	12.5	16.2	16.8	11.1	12.0	13.4

Turbomachinery Efficiency

Once the three operating points for each speed were identified, a sensitivity study around the turbomachinery efficiencies was undertaken. Figures 12-14 and Figures 15-17 show the responses to changes in turbomachinery efficiencies for the operating points, at 1500 rpm and 3000 rpm respectively. The compressor and turbine isentropic efficiencies were initially assumed to both be 70% and this serves as a baseline for the plots. The compressor isentropic efficiency was then varied (to 60% and 80%) whilst holding the turbine isentropic efficiency constant at 70%. The turbine efficiency was then varied in the same way, with the compressor efficiency being held at 70%. Figures 12 and 15 show that increased turbomachinery efficiencies lead to increased brake torque and reduced BSFC. Figures 13 and 16 demonstrate why this occurs; the increased turbomachinery efficiencies lead to increased compressor torque, in turn leading to increased brake torque for the same quantity of combusted fuel, decreasing BSFC. The increased turbomachinery efficiencies allow for a greater proportion of the work, either extracted by the turbine or imparted by the compressor, to be utilized with less losses, thus increasing the torque of the compounding system. As the compounding torque is negative for all operating points, this shows that the required work to compress the inlet gases to the desired pressure is greater than the work that can be extracted from the exhaust gases by the turbine. In this sense, the compounding system is operating like a turbocharger and supercharger in parallel. Therefore, an increase in compounding torque causes the compounding torque to become less negative. Furthermore, it can be seen that varying the compressor efficiency has a greater effect compared to varying the turbine efficiency by the same amount. This is mainly due to the compressor work being larger than the turbine work, as the resultant compounding work is negative. A ten percent change of the larger compressor work value will clearly result in a larger output change, compared to a ten percent change in the smaller turbine work value. The more negative the compounding work, the greater this effect will become. Figures 13 and 16 clearly show a larger difference between the compressor and turbine efficiency lines at operating points with more negative compounding torque. Figures 14 and 17 exemplify the linear relationship between compounding torque and BSFC, showing that further reductions in BSFC are possible by maximizing compounding torque. The authors believe that peak isentropic turbomachinery efficiencies of 80% and 75%, for the compressor and turbine respectively, could be achievable. The performance increases that these efficiencies would yield are shown in Figures 12-17. These efficiencies are used in all following simulations, with their respective results being used as a baseline for further investigations.

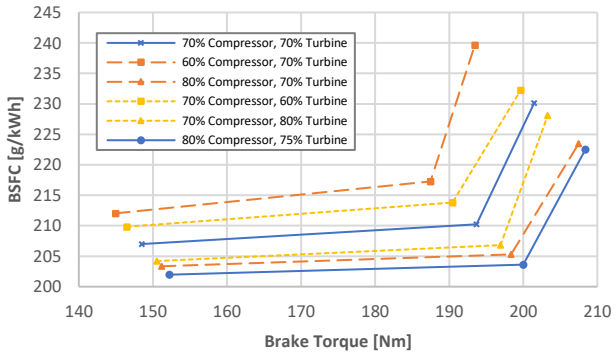

Figure 12. Effect of various compressor and turbine isentropic efficiencies on a graph of BSFC against brake torque for the 1500 rpm operating points.

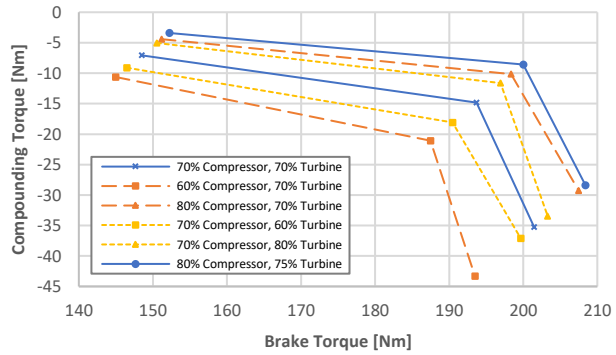

Figure 13. Effect of various compressor and turbine isentropic efficiencies on

a graph of compounding torque against brake torque for the 1500 rpm operating points.

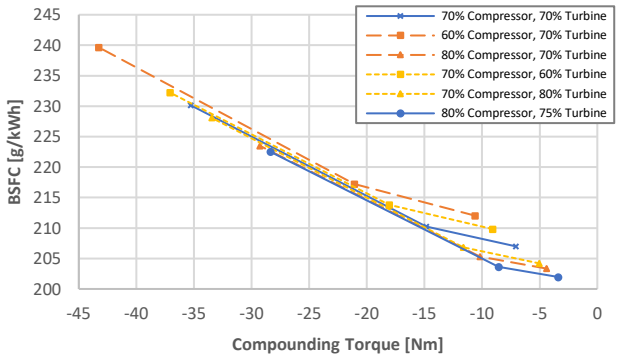

Figure 14. Effect of various compressor and turbine isentropic efficiencies on a graph of BSFC against compounding torque for the 1500 rpm operating points.

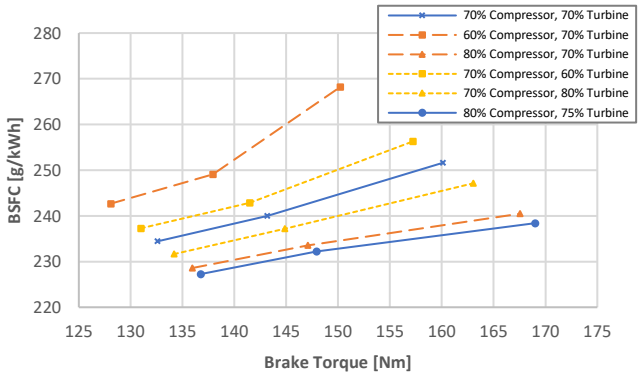

Figure 15. Effect of various compressor and turbine isentropic efficiencies on a graph of BSFC against brake torque for the 3000 rpm operating points.

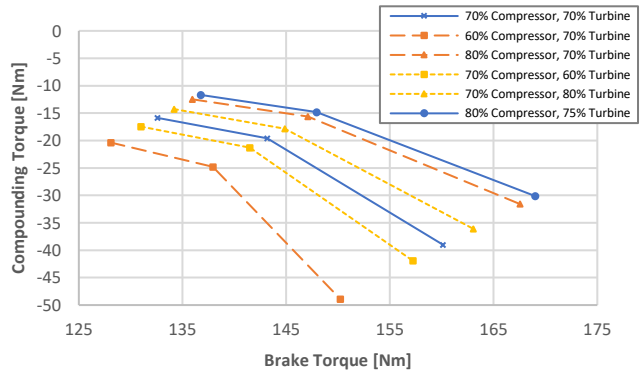

Figure 16. Effect of various compressor and turbine isentropic efficiencies on a graph of compounding torque against brake torque for the 3000 rpm operating points.

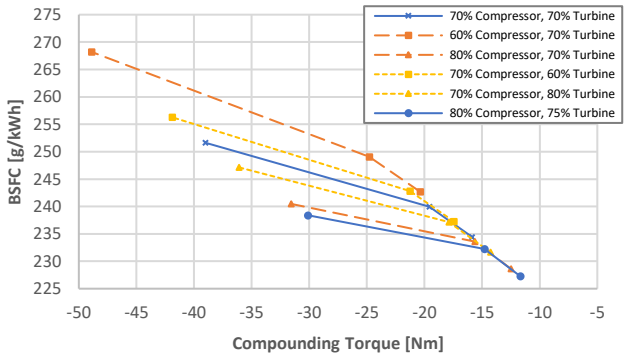

Figure 17. Effect of various compressor and turbine isentropic efficiencies on a graph of BSFC against compounding torque for the 3000 rpm operating points.

Reheat

As shown in the turbomachinery sensitivity study above, increasing the compounding torque provides a means of boosting the brake torque output of the engine whilst reducing the BSFC. A few different methodologies could be used in an attempt to maximize the compounding torque; one such method is increasing the turbine work extraction by maximizing the energy in the exhaust gases. Retarding the combustion event is known to increase the exhaust gas energy, but at the expense of reduced piston work. Adding reheat functionality provides another means of increasing the exhaust gas energy but without impacting the piston work. As all operating points are lean, excess free oxygen is present in the exhaust gases; this allows for a further combustion event to occur within the exhaust system (before the turbine) to increase the gas energy. This is assumed to occur within the close coupled pre-turbine catalyst yielding the benefits of catalytic combustion. For each operating point, the mass fraction of oxygen in the exhaust gases determines the quantity of fuel that can be combusted to achieve stoichiometric products. This is termed '100% potential reheat' with '50% potential reheat' referring to half this value. The combustion event will raise the exhaust gas temperature, yielding greater work extraction by the turbine. A temperature limit of 1273K is set to protect the turbine. If this limit is reached, only the quantity of fuel required to achieve the 1273K exhaust gas temperature limit will be used.

Table 5. Summary of the reheat calculations for the three operating points at each engine speed.

		1500 rpm			3000 rpm		
Operating Point		**A**	**B**	**C**	**A**	**B**	**C**
Cylinder Fuel Mass Flow Rate [g/s]		1.34	1.78	2.02	2.71	3.00	3.52
Mass Fraction of O_2 [%]		2.88	2.78	6.79	1.08	0.59	2.04
Initial Exhaust Gas Temperature[K]		820	819	743	935	934	870
50% Potential	**Reheat Fuel Mass Flow Rate [g/s]**	0.12	0.16	0.48	0.08	0.05	0.22
	Achievable Temp. Increase [K]	143	138	349	52.1	28.3	100
	New Exhaust Gas Temperature [K]	963	957	1092	987	962	970
100 %	**Reheat Mass Fuel Flow Rate [g/s]**	0.25	0.31	0.73	0.15	0.09	0.44

	Achievable Temp. Increase [K]	286	276	698	104	57	200
	New Exhaust Gas Temperature [K]	1106	1095	1273	1039	991	1070

Table 4 summarizes the aforementioned calculations for each operating point. The cylinder fuel mass flow rates are included for comparison with the calculated reheat fuel mass flow rates. The exhaust oxygen mass fractions are higher for all 1500 rpm operating points compared to those for 3000 rpm. This, in part, is due to the leaner operation of the engine in general at 1500 rpm; however, the especially high value for 1500 rpm, operating point C is believed to be due to charge 'short circuiting' (where fresh charge passes through into the exhaust system during valve overlap before combustion). Due to the high exhaust oxygen mass fraction at this operating point, the 1273K temperature limit is reached during '100% potential reheat', limiting the reheat fuel flow rate; this does not occur for any other operating point. Figures 18-20 and Figures 21-23 show the effect of reheat on the operating points for 1500 rpm and 3000rpm respectively. Figure 18 demonstrates that the addition of reheat leads to increased brake torque due to the increased compounding torque, as seen in Figure 19, but at the expense of increased BSFC. Operating points A and B show positive compounding torque when using 100% potential reheat. However, even though operating point B, under 100% potential reheat, has positive compounding torque, it yields a brake torque only marginally larger (2 Nm) than operating point C, with no reheat, with a much increased BSFC (17 g/kWh). This exemplifies the fuel inefficiency of this reheat system, showing how little of the fuel energy ends up increasing the brake torque of the engine. Figure 20 provides further evidence of this, with operating points that show a greater compounding torque increase having the largest BSFC increase. Nevertheless, the use of reheat has yielded the first example of positive compounding torque, providing initial proof that turbocompounding the OP2S engine could be feasible.

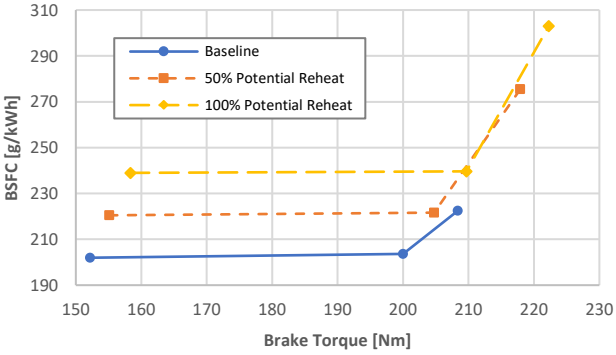

Figure 18. Effect of different levels of reheat on a graph of BSFC against brake torque for the 1500 rpm operating points.

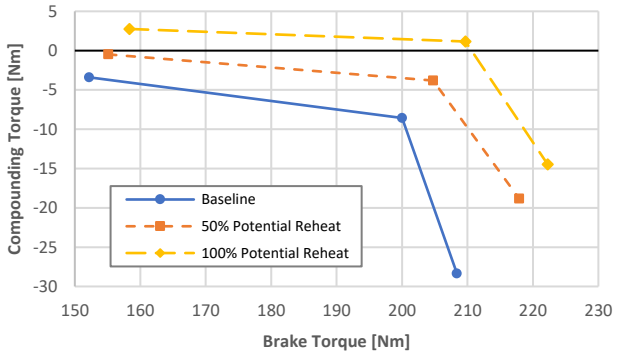

Figure 19. Effect of different levels of reheat on a graph of compounding torque against brake torque for the 1500 rpm operating points.

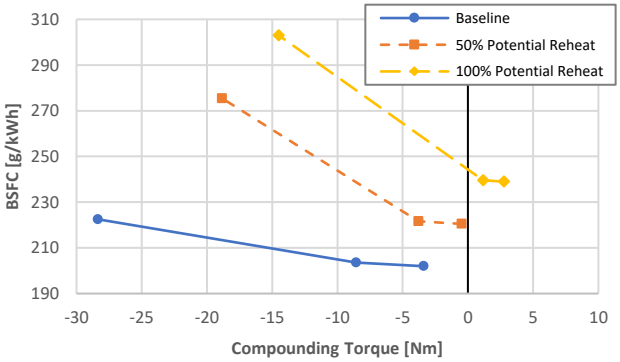

Figure 20. Effect of different levels of reheat on a graph of BSFC against compounding torque for the 1500 rpm operating points.

Similar trends can be seen in Figures 21-23 for the 3000 rpm operating points, albeit to lesser degree due to the lower mass fractions of oxygen in the exhaust gases. Figure 21 further demonstrates the fuel inefficiency of the reheat system by causing the line of operating points to change from a peaked center to a valleyed center, due to operating point B having the lowest mass fraction of oxygen and thus the lowest amount of potential reheat fuel flow. The effect is especially apparent in Figure 23. Figure 22 shows very little difference in the values for operating points A and B between 50% and 100% potential reheat, suggesting that the effect could be non-linear. However, it is believed that this is due to minor errors in the assumptions made surrounding the effects of reheat on the exhaust specific heat capacity and specific heat ratio.

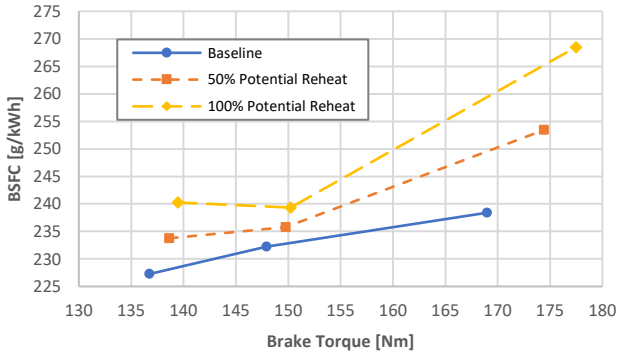

Figure 21. Effect of different levels of reheat on a graph of BSFC against brake torque for the 3000 rpm operating points.

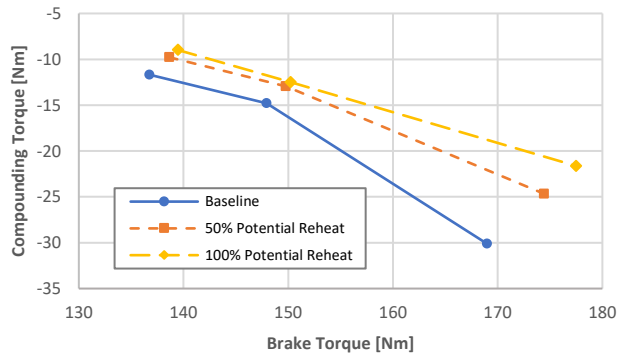

Figure 22. Effect of different levels of reheat on a graph of compounding torque against brake torque for the 3000 rpm operating points.

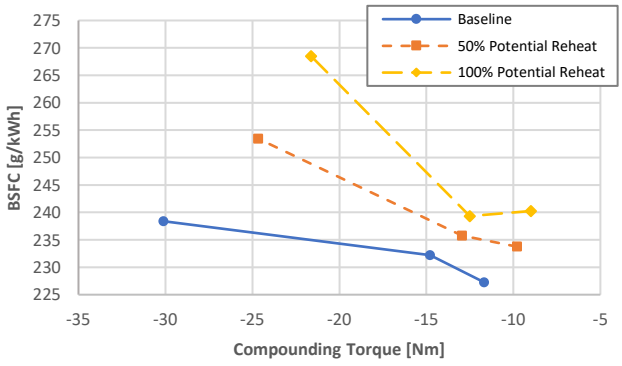

Figure 23. Effect of different levels of reheat on a graph of BSFC against compounding torque for the 3000 rpm operating points.

Backpressure

The exhaust backpressure caused by the aftertreatment and muffler system is estimated in the model using an approximated pressure drop that varies with the square of volumetric exhaust gas flow rate. A constant of proportionality is used to scale the pressure drop to typical values expected from this type of engine, from the authors' experiences. However, as this is an approximation, the actual backpressures seen during engine operation could vary, depending on a number of factors. Furthermore, the flow restriction, and thus the pressure drop, that the aftertreatment and muffler present can be considered as a design constraint to be used during the exhaust system design process. As the use of a close coupled pre-turbine catalyst is proposed in this work, the flow restriction of the post-turbine aftertreatment system could be reduced, yielding less backpressure. Therefore, the ability to evaluate the effects of changing the exhaust backpressure provides functionality for future optimization of the aftertreatment and muffler systems. For the purpose of demonstrating the effects of this functionality, two levels of backpressure reduction have been modelled: '50% reduced backpressure' and 'no backpressure'. The '50% reduced backpressure' refers to a halving of the calculated pressure drops for each operating point baseline. 'No backpressure' means that no pressure drop occurs, suggesting no aftertreatment or muffler system is in place, so the post-turbine pressure is 1 bar absolute; this is representative of engines used in aircraft applications or Formula 1.

Table 6. Summary of the backpressure values used in the simulations for the three operating points at each engine speed.

	1500 rpm			**3000 rpm**		
Operating Point	**A**	**B**	**C**	**A**	**B**	**C**
Exhaust Mass Flow Rate [g/s]	30.0	39.7	49.8	50.3	54.7	76.3
Baseline Backpressure [bar]	1.16	1.28	1.45	1.46	1.54	2.05
50% Reduced Backpressure [bar]	1.08	1.14	1.22	1.23	1.27	1.52
No Backpressure [bar]	1.00	1.00	1.00	1.00	1.00	1.00

Table 5 summarizes the backpressure values used for each operating point, at each backpressure level. Figures 24-26 and Figures 27-29 show the effects of varying the exhaust backpressure on the performance of the operating points at 1500 rpm and 3000 rpm respectively. Figure 24 demonstrates that reducing backpressure increases brake torque but, conversely to reheat, reduces the BSFC, as extra torque is made available without combusting anymore fuel. The increase in brake torque, once again, arises from the increased compounding torque, as shown in Figure 25. Operating point A with no backpressure was the only point to yield positive compounding torque, albeit only 0.3 Nm, with operating point B narrowly missing out at -0.3 Nm. When compared to the compounding torque values for 100% potential reheat of 2.8 Nm and 1.2 Nm for operating points A and B respectively, the effect of reducing backpressure is clearly inferior, if maximizing compounding torque is the primary aim. This is to be predicted as the low exhaust flow rates at these operating points cause low backpressure values. However, it must be noted that, even though the effects of reducing exhaust backpressure on compounding torque at 1500 rpm are more slight, they are accompanied with the benefit of decreased BSFC. The effect of increased compounding torque with reduced backpressure become more apparent as the exhaust gas flow rate increases, due to the larger reduction in backpressure that occurs. Figure 26, along with the other two figures, show that the effects of reducing backpressure on brake torque, compounding torque and BSFC are linear.

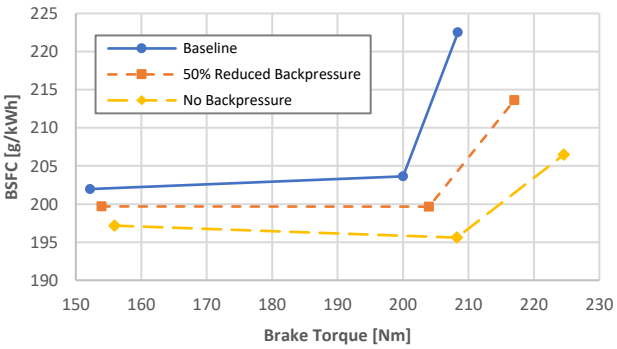

Figure 24. Effect of different levels of backpressure on a graph of BSFC against brake torque for the 1500 rpm operating points.

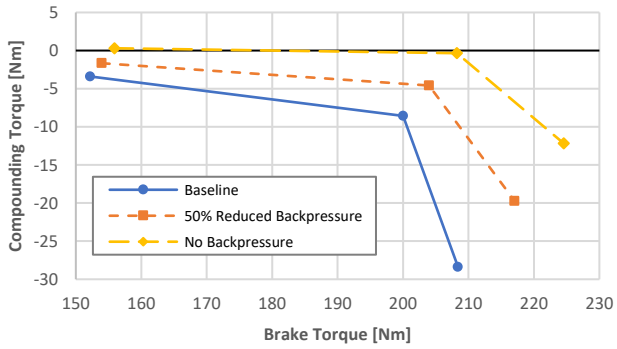

Figure 25. Effect of different levels of backpressure on a graph of compounding torque against brake torque for the 1500 rpm operating points.

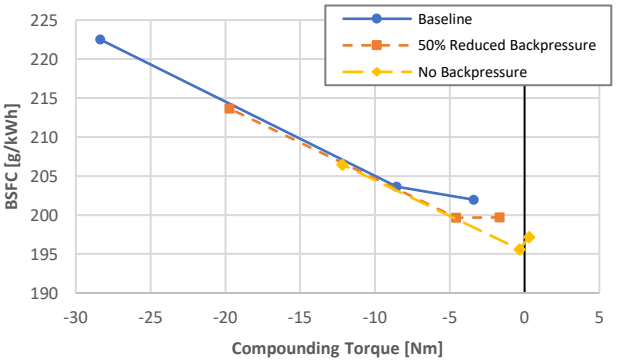

Figure 26. Effect of different levels of backpressure on a graph of BSFC against compounding torque for the 1500 rpm operating points.

Figure 27 displays that similar trends occur at 3000 rpm, with an increase in brake torque and decrease in BSFC occurring with reduced backpressure. Even though, on average, the increase in compounding torque at 3000 rpm is twice that at 1500 rpm, due to the increased exhaust mass flow rates, no 3000 rpm operating points yield positive compounding torque. However, as seen in Figure 28, all three 'no backpressure' operating points have compounding torque values greater than -5 Nm, indicating that it could be possible to achieve positive compounding torque from all three. The sensitivities of BSFC to compounding torque, and compounding torque to backpressure are apparent in Figure 29. At each backpressure step, the BSFC of each operating point is lower than every value from the previous step, due to the large gains in compounding torque that are made. Operating point C shows the greatest improvements due to the high exhaust flow rate causing very high initial backpressure.

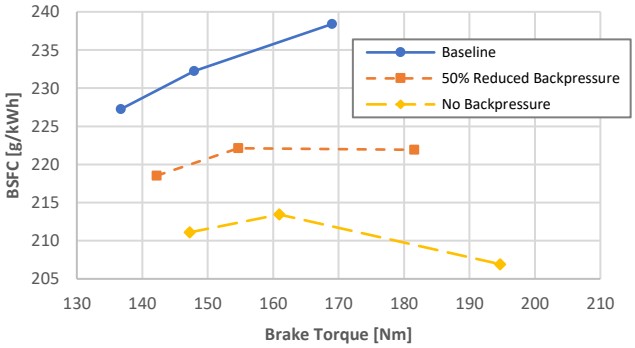

Figure 27. Effect of different levels of backpressure on a graph of BSFC against brake torque for the 3000 rpm operating points.

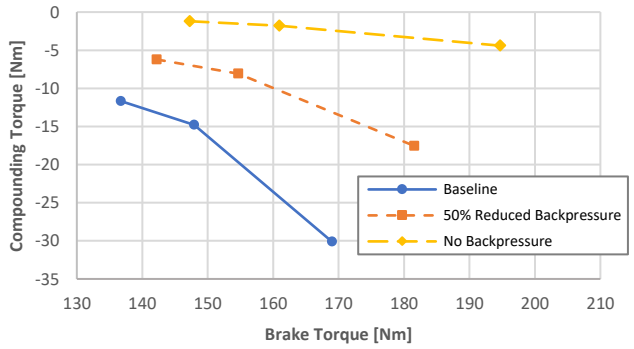

Figure 28. Effect of different levels of backpressure on a graph of compounding torque against brake torque for the 3000 rpm operating points.

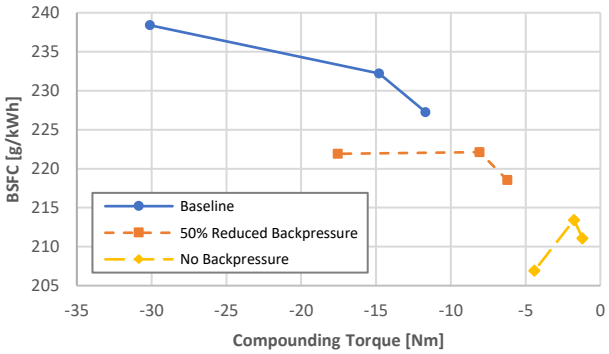

Figure 29. Effect of different levels of backpressure on a graph of BSFC against compounding torque for the 3000 rpm operating points.

Reheat and Backpressure

It is clear that reheat suited the 1500 rpm operating points more due to the better scavenging performance and leaner engine operation, both of which served to increase the mass fraction of oxygen in the exhaust

gases. Conversely, reducing backpressure suited the 3000 rpm operating points more due to the increased exhaust mass flow rates yielding higher initial backpressure values. Therefore, it could be beneficial for overall engine performance to utilize a combination of both. Figures 30-32 and Figures 33-35 demonstrate the combined effects of reheat and backpressure on the operating points for 1500 rpm and 3000 rpm respectively. The same baseline values are used along with the combined 50% and 100% steps. As both reheat and backpressure increase compounding torque, the combined effect is substantial, as can be seen in Figures 31-32 where all operating points for 100% reheat with no backpressure yield positive compounding torque; 5% to 6% of the brake torque under these conditions is provided by the compounding system. Furthermore, operating points A and B for 50% reheat and 50% reduced backpressure also yield positive compounding work, albeit both less than 2 Nm. The increased brake torque caused by the increased compounding torque is also shown. Figure 30 shows that the improvement in BSFC from the reduction of backpressure is overpowered by the increased fuel usage during reheat, resulting in a net increase in BSFC when combined. However, it can be seen that, for operating point C, an increase in brake torque of over 20 Nm can be achieved with an increase in BSFC of less than 1 g/kWh, between '50% reheat, 50% reduced backpressure' and '100% reheat, no backpressure'. Furthermore, operating point B with 50% reheat and 50% reduced backpressure yields a 1 Nm greater brake torque with an 11 g/kWh reduced BSFC compared to the baseline operating point C.

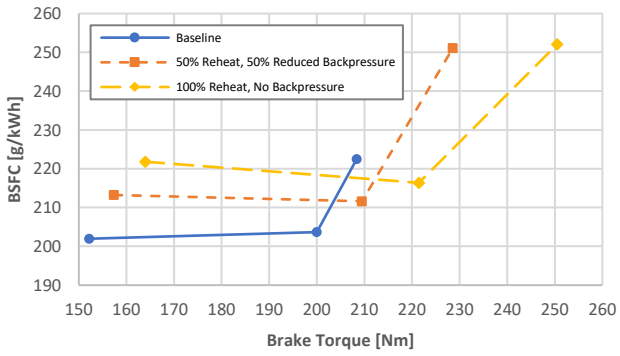

Figure 30. Effect of different levels of combined reheat and backpressure on a graph of BSFC against brake torque for the 1500 rpm operating points.

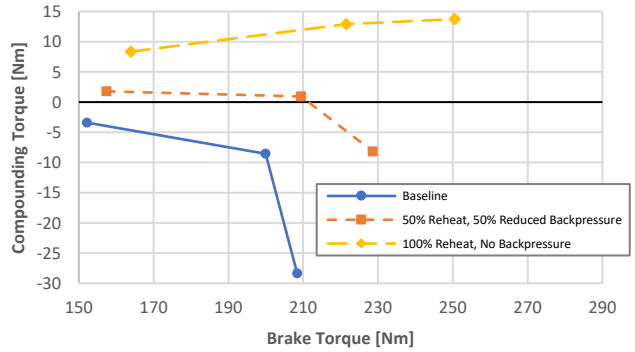

Figure 31. Effect of different levels of combined reheat and backpressure on a graph of compounding torque against brake torque for the 1500 rpm operating points.

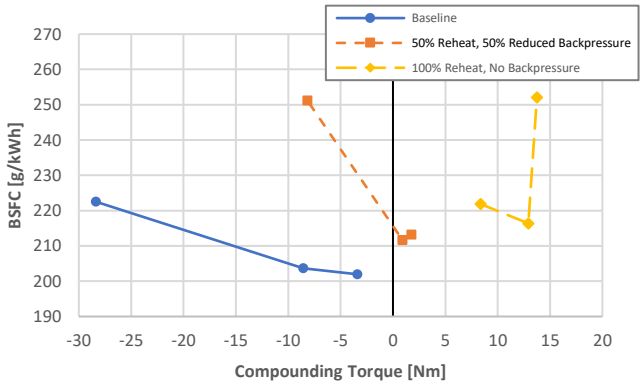

Figure 32. Effect of different levels of combined reheat and backpressure on a graph of BSFC against compounding torque for the 1500 rpm operating points.

Once again, increased compounding torque yields increased brake torque, demonstrated in Figure 33. However, in contrast to 1500 rpm, the BSFC improvement from the reduced backpressure at 3000 rpm dominates the increased fuel usage by reheat, yielding a net decrease in BSFC when combined. Figure 35 demonstrates just how dominant this is, with all operating points at '100% reheat, no backpressure' having the lowest BSFCs. Figure 34 shows that all 3000 rpm operating points with 100% reheat and no backpressure yield positive compounding torque, showing that net positive compounding work is possible for all operating points at 3000 rpm.

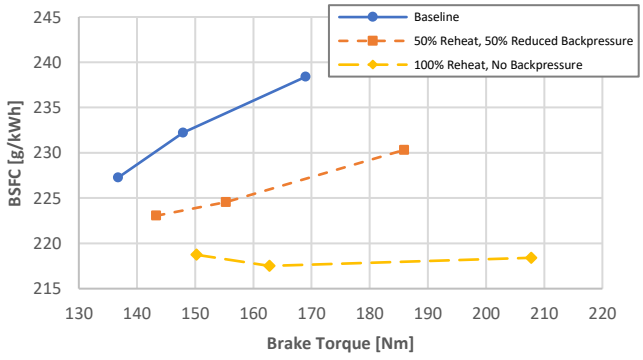

Figure 33. Effect of different levels of combined reheat and backpressure on a graph of BSFC against brake torque for the 3000 rpm operating points.

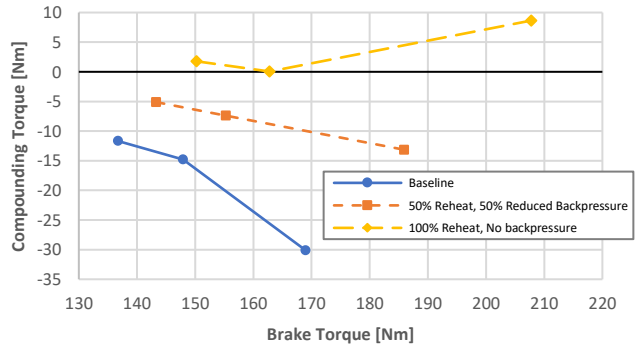

Figure 34. Effect of different levels of combined reheat and backpressure on a graph of compounding torque against brake torque for the 3000 rpm operating points.

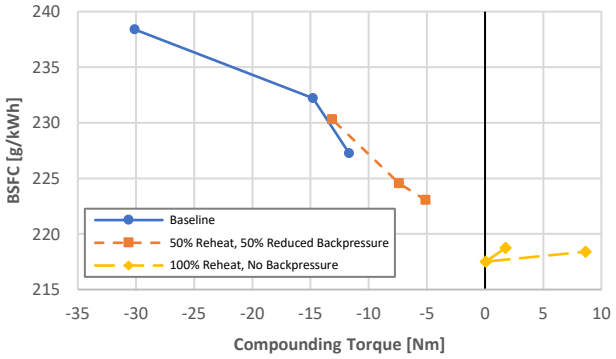

Figure 35. Effect of different levels of combined reheat and backpressure on a graph of BSFC against compounding torque for the 3000 rpm operating points.

Conclusions and Further Work

The suitability of turbocompounding the OP2S engine has been assessed, at 1500 rpm and 3000 rpm, using a 1-D engine simulation software. An optimizer, assigned to target maximum brake torque, maximum compounding torque and minimum BSFC, was used to parameterize the chosen input variables. Three operating points (A: high compounding torque; B: efficiency knee; C: peak torque), for each engine speed, were chosen from the optimizer results and used in the subsequent studies. These involved assessing the effects of turbomachinery efficiencies, reheat and backpressure.

The conclusions drawn from this work were:

1. Increased turbomachinery efficiencies lead to increased brake torque and decreased BSFC by virtue of increased compounding torque. Varying the compressor efficiency has a greater effect compared to the turbine efficiency as the net compounding torque was negative, meaning that the compressor work was greater than the turbine work.
2. The addition of reheat showed increased brake torque due to the increased compounding torque but at the expense of increased BSFC. Using 100% potential reheat allowed for operating points A and B at 1500 rpm to yield positive compounding torque values. The effects at 3000 rpm were similar but to a lesser degree due to the lower mass fraction of oxygen in the exhaust gases from poorer engine scavenging and richer engine operation.
3. The reduction of exhaust backpressure led to increased brake torque and decreased BSFC due to the increased compounding torque. Even though the effects were greater at 3000 rpm, due to the higher exhaust gas flow rates causing higher initial backpressure values, the increases in compounding torque were not great enough to yield positive values for any of the operating points. The effects at 1500 rpm were slighter but nevertheless operating point A with no backpressure achieved positive compounding torque.
4. Combining the effects of reheat and reduced backpressure proved effective at maximizing compounding torque at both engine speeds. At 1500 rpm, the increased fuel consumption due to reheat dominated the BSFC reduction caused by the decreased backpressure resulting in a net increase in BSFC. However, with 100% reheat and no backpressure, positive compounding torque was achieved at all three operating points, with 5-6% of the brake torque coming from the compounding system. At 3000 rpm, the increased fuel consumption from reheat was dominated by the backpressure reduction resulting in a net decrease in BSFC. Positive compounding torque was also achieved at all three operating points with 100% reheat and no backpressure. The maximum percentage of brake torque supplied by the compounding system at 3000 rpm was 4%.

These results demonstrate that turbocompounding the OP2S engine is feasible and could be a viable option for waste heat energy recovery; however, positive compounding work has only been demonstrated under certain operating conditions. This is believed to be due to limitations caused by the engine geometries, port open areas, scavenging, etc. These were all established in a prior work with an optimizer being used to minimize specific fuel consumption at 1500 rpm. This is apparent in the comparatively poorer performance at 3000 rpm throughout this work. It is suggested that, with the new model developments, further optimization of the engine geometries should be undertaken, which may yield an improved propensity for turbocompounding. Furthermore, the OP2S engine can be operated with variable compression ratio by changing the phasing of the pistons; it is recommended that this effect and its impact on engine performance should be investigated.

References

1. Jones, L., Sectioned drawings of Piston Aero Engines, Historical Series Special Edition (Derby, UK: Rolls-Royce Heritage Trust, 1995). ISBN:1 872922 07 4.
2. Pearce, W., Junkers Jumo 223 Aircraft Engine, (Old Machine Press), available at https://oldmachinepress.com/2015/09/26/junkers-jumo-223-aircraft-engine/, last accessed 28th November 2020.
3. Pearce, W., Junkers Jumo 224 Aircraft Engine, (Old Machine Press), available at https://oldmachinepress.com/2015/10/03/junkers-jumo-224-aircraft-engine/, last accessed 28th November 2020.
4. Regner, G., Herold, R.E., Wahl, M.H., Dion, E. et al., "The Achates Power Opposed-Piston Two-Stroke Engine: Performance and Emissions Results in a Medium-Duty Application," SAE Int. J. Engines 4(3):2726-2735, 2011, doi:10.4271/2011-01-2221.
5. Redon, F., Kalebjian, C., Kessler, J., Rakovec, N. et al., "Meeting Stringent 2025 Emissions and Fuel Efficiency Regulations with an Opposed-Piston, Light-Duty Diesel Engine," SAE Technical Paper 2014-01-1187, 2014, doi:10.4271/2014-01-1187.
6. Sharma, A. and Redon, F., "Multi-Cylinder Opposed-Piston Engine Results on Transient Test Cycle," SAE Technical Paper 2016-01-1019, 2016, doi:10.4271/2016-01-1019.
7. Naik, S., Johnson, D., Fromm, L., Koszewnik, J. et al., "Achieving Bharat Stage VI Emissions Regulations While Improving Fuel Economy with the Opposed-Piston Engine," SAE Int. J. Engines 10(1):17-26, 2017, doi:10.4271/2017-26-0056.
8. Witzky, J., Meriwether, R., and Lux, F., "Piston-Turbine-Compound Engine — A Design and Performance Analysis," SAE Technical Paper 650632, 1965, doi:10.4271/650632
9. Nahum, A., Foster-Pegg, R.W., and Birch, D., The Rolls-Royce Crecy, Rolls-Royce Heritage Trust Historical Series No. 21 (Derby, UK: Rolls-Royce Heritage Trust, 1994). ISBN:1 872922 05 8.
10. Chatterton, E., "The Napier Deltic Diesel Engine," SAE Technical Paper 560038, 1956, doi:10.4271/560038.

11. Aghaali, H., Ångström H., “A review of turbocompounding as a waste heat recovery system for internal combustion engines.” Renewable and Sustainable Energy Reviews, Volume 49, 2015, Pages 813-824, ISSN 1364-0321, doi:10.1016/j.rser.2015.04.144.
12. Wei, W., Zhuge, W., Zhang, Y., & He, Y., "Comparative Study on Electric Turbo-Compounding Systems for Gasoline Engine Exhaust Energy Recovery." Proceedings of the ASME Turbo Expo 2010: Power for Land, Sea, and Air. Volume 5: Industrial and Cogeneration; Microturbines and Small Turbomachinery; Oil and Gas Applications; Wind Turbine Technology. Glasgow, UK. June 14–18, 2010. pp. 531-539. doi:10.1115/GT2010-23204.
13. Kant, M., Romagnoli, A., Mamat, A. M., & Martinez-Botas, R. F., “Heavy-Duty Engine Electric Turbocompounding.” Proceedings of the Institution of Mechanical Engineers, Part D: Journal of Automobile Engineering 229, no. 4 (March 2015): 457–72. doi:10.1177/0954407014547237.
14. Turner, J.W.G., Head, R.A., Chang, J., Engineer, N. et al., “2-Stroke Engine Options for Automotive Use: A Fundamental Comparison of Different Potential Scavenging Arrangements for Medium-Duty Truck Applications,” SAE Technical Paper 2019-01-0071, 2019, doi:10.4271/2019-01-0071.
15. Badra, J.A., Sim, J., Elwardany, A., Jaasim, M. et al., “Numerical Simulations of Hollow-Cone Injection and Gasoline Compression Ignition Combustion with Naphtha Fuels,” Journal of Energy Resources Technology 138(5), February 2016, doi:10.1115/1.4032622.
16. Mattarelli, E., Rinaldini, C., Savioli, T., Cantore, G. et al., “Scavenge Ports Optimization of a 2-Stroke Opposed Piston Diesel Engine,” SAE Technical Paper 2017-24-0167, 2017, doi:10.4271/2017-24-0167.
17. Subramaniam, M., “Pre-turbo After-treatment System Development using a 1D Modeling Approach.” Retrieved from https://www.fev.com/fileadmin/user_upload/Media/TechnicalPublications/Diesel_Systems/PreturboAfterTreatmentSystemwitha1DModelingApproach.pdf.
18. Catalysts - AECC - From oxidation catalysts to three-way catalysts. (2020, November 19). Retrieved December 02, 2020, from https://www.aecc.eu/emissions-control-technology/catalysts/.
19. Parsons, D., “The Effect of Post-Catalyst Exhaust Gas Recirculation on Combustion in Highly Rated SI Engines.” 15 Jan 2020, Student thesis: Doctoral Thesis › PhD.
20. Kalghatgi, G., Risberg, P., and Ångström, H., "Advantages of Fuels with High Resistance to Auto-ignition in Late-injection, Low-temperature, Compression Ignition Combustion," SAE Technical Paper 2006-01-3385, 2006, doi:10.4271/2006-01-3385.
21. Kalghatgi, G., & Johansson, B., “Gasoline Compression Ignition Approach to Efficient, Clean and Affordable Future Engines.” Proceedings of the Institution of Mechanical Engineers, Part D: Journal of Automobile Engineering 232, no. 1 (January 2018): 118–38. doi:10.1177/0954407017694275.
22. Agarwal, A.K., Singh, A.P., Maurya, R.K., “Evolution, challenges and path forward for low temperature combustion engines,” Progress in Energy and Combustion Science, Volume 61, 2017, Pages 1-56, ISSN 0360-1285, doi.org/10.1016/j.pecs.2017.02.001.
23. AlAbbad, M., Badra, J., Djebbi, K., Farooq, A., “Ignition delay measurements of a low-octane gasoline blend, designed for gasoline compression ignition (GCI) engines,” Proceedings of the Combustion Institute, Volume 37, Issue 1, 2019, Pages 171-178, ISSN 1540-7489, doi.org/10.1016/j.proci.2018.05.097.
24. He, X., Donovan, M.T., Zigler, B.T., Palmer, T.R. et al., “An experimental and modeling study of iso-octane ignition delay times under homogeneous charge compression ignition conditions,” Combustion and Flame, Volume 142, Issue 3, 2005, Pages 266-275, ISSN 0010-2180, doi:10.1016/j.combustflame.2005.02.014.
25. Regner, G., Redon, F., Koszewnik, J., & Fromm, L. et al. “Achieving the Most Stringent CO2 Commercial Truck Standards with Opposed Piston Engine.” Retrieved from https://achatespower.com/wp-content/uploads/2019/12/MTZ_2014_Final.pdf.
26. Yoshizawa, K., Teraji, A., Miyakubo, H., Yamaguchi, K. et al. “Study of High Load Operation Limit Expansion for Gasoline Compression Ignition Engines.” ASME. J. Eng. Gas Turbines Power. April 2006; 128(2): 377–387. doi:10.1115/1.1805548.
27. Liu, H., Mao, B., Liu, J., Zheng, Z. et al. "Pilot injection strategy management of gasoline compression ignition (GCI) combustion in a multi-cylinder diesel engine," Fuel, Volume 221, 2018, Pages 116-127, ISSN 0016-2361, doi:10.1016/j.fuel.2018.01.073.

Contact Information

Alexander George Young
AAPS CDT PhD Student
Department of Mechanical Engineering
University of Bath
Claverton Down
Bath BA2 7AY
United Kingdom
agy22@bath.ac.uk

Acknowledgments

Alex is supported by a scholarship from the EPSRC Centre for Doctoral Training in Advanced Automotive Propulsion Systems (AAPS), under the project EP/S023364/1.
Funding from Saudi Aramco to conduct the original 2-stroke scavenging work is gratefully acknowledged.

Definitions/Abbreviations

1-D	One-dimensional
AFR	Air-fuel ratio
ATDC	After top dead centre
BMEP	Brake mean effective pressure
BSFC	Brake specific fuel consumption
CA50	50% burned crank angle
CAC	Charge air cooler
CAD	Crank angle degrees

EAT	Exhaust aftertreatment
EGR	Exhaust gas recirculation
EM	Electric machines
FMEP	Friction mean effective pressure
GCI	Gasoline compression ignition
HC	Hydrocarbon
IMEP	Indicated mean effective pressure
MAP	Manifold absolute pressure
MPRR	Maximum pressure rise rate
NVH	Noise, vibration and harshness
OP2S	Opposed-piston 2-stroke
SOI	Start of injection